Uncalibrated photometric stereo constrained by intrinsic reflectance image and shape from silhoutte

Shuhei Hashimoto   Daisuke Miyazaki   Shinsaku Hiura

miyazaki@hiroshima-cu.ac.jp

Hiroshima City University

3-4-1 Ozukahigashi, Asaminami-ku, Hiroshima, 731-3194 JAPAN

Abstract

Photometric stereo is a method which estimates surface normal from object's shading. Uncalibrated photometric stereo is the photometric stereo where the light source direction is unknown. Uncalibrated photometric stereo which estimates both light source direction and surface normal is an ill-posed problem, and has ambiguity for solving the problem. In order to uniquely determine the solution, constraints should be added. Two constraints we use are the intrinsic image which represents the albedo (diffuse reflectance) and the guide normal which represents the approximate shape of the object. Estimation of albedo requires both the normal and the light direction to be known, but both are unknown in our situation. Our method employs the idea of intrinsic image decomposition, and estimates the reflectance solely from input image sequence. In addition, we estimate the approximate shape from images without using other sensors such as laser range sensor. This paper reveals that the uncalibrated photometric stereo can be solved by these two constraints.

1   Introduction

Uncalibrated photometric stereo which allows the light source directions to be unknown has ambiguity in uniquely determining the solution. In order to solve the problem, we use the intrinsic reflectance image and approximate normal as the constraints.

Shading is consisted of albedo (diffuse reflectance), surface normal, and light source direction. The albedo, the surface normal, and the light direction (of infinite-far point light source) are all unknown in our situation (Figure 1). In order to solve the problem, we constrain the albedo and the normal. The approximate estimate of albedo is calculated solely from input images using the idea employed in the field of intrinsic image decomposition. The approximate estimate of normal is calculated solely from input images using the silhouette of object region. However, these two estimates are not that correct. In order to survive this severe situation, we use the framework of uncalibrated photometric stereo, which works stably for this severe situation.
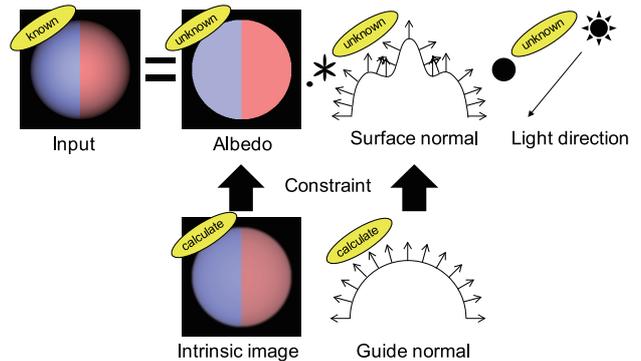

Figure 1. Uncalibrated photometric stereo constrained by intrinsic reflectance image and shape from silhoutte.

2   Related works

The photometric stereo under the condition that the light source direction is unknown is called uncalibrated photometric stereo [25, 10, 28, 1, 4, 19, 3, 18, 6, 9, 5, 1, 29, 7, 27].

Generally, uncalibrated photometric stereo has a problem that it is sensitive to outliers such as specular reflection and shadow. Photometric linearization [17, 23, 20, 26, 11, 16, 15, 22, 11] is useful to be applied a priori. Photometric linearization is out of scope of this paper, thus we do not treat with this problem but we use these techniques as preprocessing of our method.

Intrinsic image decomposition [13, 2, 12, 21, 8, 24, 14] is an method which decomposes an image into two intrinsic images which represent illumination and reflectance (Figure 2). It is an ill-posed problem to both estimate the illumination environment and the object shape under the condition that both are unknown. In most cases, it is solved by adding an assumption derived from the statistical property of images. We borrow the idea examined in the field of intrinsic image decomposition, and apply the modified version of the idea so that it can be applied to uncalibrated photometric stereo.

Hayakawa [10] proved that uncalibrated photometric stereo can be solved if the albedo of the object (*or*

the brightness of light source) is uniform. Corollary 4.1 given by Belhumeur *et al.* [4] also proved this fact. In order to treat with objects with multiple albedos, we calculate the intrinsic image which represents the albedo. Proposed method cancels the albedo at the first stage of the algorithm, which increases the robustness of our method since the succeeding processes becomes simple.

3 Uncalibrated photometric stereo

3.1 Lambert reflection

Under the condition that the object obeys the Lambertian reflection model and the light source is an infinite-far single light, the observed brightness i can be represented as follows.

$$i = \mathbf{s} \cdot \mathbf{l}, \tag{1}$$

where the vector $\mathbf{s} = (s_x, s_y, s_z)^\top$ is called surface vector and the unit vector $\mathbf{l} = (l_x, l_y, l_z)^\top$ is called light vector. Surface vector $\mathbf{s}$ is a product of albedo and normal vector. Light vector $\mathbf{l}$ represents the light source direction.

Since $\mathbf{s} \cdot \mathbf{l}$ might become negative, Equation (1) is usually formulated as $i = \max(\mathbf{s} \cdot \mathbf{l}, 0)$. However, the photometric linearization [17, 23, 20, 26, 11, 16, 15] forces the images to obey Equation (1). The photometric linearization is applied to the captured images, and such images are used as inputs of our method. Recent methods often use LASSO [22, 11] but any other equivalent methods can be used. We employ the robust SVD [23, 20, 16, 15] in this work.

Following shows the $P \times 3$ surface matrix which is a concatenation of surface vectors and the $3 \times F$ light matrix $\mathbf{L}$ which is a concatenation of light vectors, where P represents the number of pixels and F represents the number of images.

$$\mathbf{S} = \begin{pmatrix} s_{1x} & s_{1y} & s_{1z} \\ s_{2x} & s_{2y} & s_{2z} \\ \vdots & \vdots & \vdots \\ s_{Px} & s_{Py} & s_{Pz} \end{pmatrix}, \tag{2}$$

$$\mathbf{L} = \begin{pmatrix} l_{x1} & l_{x2} & \ldots & l_{xF} \\ l_{y1} & l_{y2} & \ldots & l_{yF} \\ l_{z1} & l_{z2} & \ldots & l_{zF} \end{pmatrix}. \tag{3}$$

Input data is represented by following matrix I.

$$\mathbf{I} = \mathbf{S}\mathbf{L} = \begin{pmatrix} i_{11} & i_{12} & \ldots & i_{1F} \\ i_{21} & i_{22} & \ldots & i_{2F} \\ \vdots & \vdots & \ddots & \vdots \\ i_{P1} & i_{P2} & \ldots & i_{PF} \end{pmatrix}. \tag{4}$$

Since the rank of both the surface matrix $\mathbf{S}$ and the light matrix $\mathbf{L}$ are 3, Equation (4) implies that the rank of the matrix $\mathbf{I}$ is also 3.
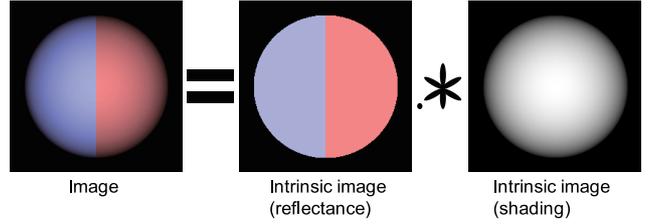

Figure 2. Intrinsic image decomposition.

3.2 Estimate of albedo

As is shown in Figure 1, the problem can be hinted by an expected albedo. Our method does not require additional sensors, thus we use the idea of intrinsic image decomposition (Figure 2) in order to estimate the albedo solely from images. Among various approaches in intrinsic image decompositions, our method employs the assumption that the albedo is constant except for the edges where the albedo might change.

First, we calculate the average image $\mathbf{a}$ which is the average of F number of images $\mathbf{i}_f$. The shade and shadow are decreased since the average image represents the image which is illuminated by multiple lights, and thus it is useful to be used as a hint to calculate the albedo.

Small amount of shading effect remains in the average image $\mathbf{a}$, thus we apply bilateral filter to the average image $\mathbf{a}$ in order to obtain the estimate of the albedo $\hat{\mathbf{a}}$. Bilateral filter is an edge-preserved smoothing filter, and thus it can be used to calculate the hypothesis to the albedo.

The obtained albedo is similar to the true albedo but is not exactly true. In order to estimate the surface normal robustly, we use the framework of uncalibrated photometric stereo in the subsequent sections since the uncalibrated photometric stereo is a powerful tool which can estimate the surface normal even under the severe condition we treat with.

3.3 Singular value decomposition

Intrinsic illumination image can be obtained by dividing an input image by an albedo (Figure 2). This paper denotes intrinsic illumination image as shading image. Shading image $\hat{i}_{pf}$ is calculated as follows, where the pixel brightness of the f-th image and the p-th pixel is represented as i_{pf} .

$$\hat{i}_{pf} = \frac{i_{pf}}{\hat{a}_p} . \tag{5}$$

Note that Equation (5) is calculated only when the estimated albedo $\hat{a}_p$ is larger than the threshold T_a.

$$\hat{a}_p > T_a . \tag{6}$$

Suppose that the number of pixels which satisfies Equation (6) is $\hat{P}$. We call the following matrix $\hat{\mathbf{I}}$ image matrix, where the pixels of the shading image is located vertically and the images are located horizontally.

$$\hat{\mathbf{I}} = \begin{pmatrix} \hat{i}_{11} & \hat{i}_{12} & \dots & \hat{i}_{1F} \\ \hat{i}_{21} & \hat{i}_{22} & \dots & \hat{i}_{2F} \\ \vdots & \vdots & \ddots & \vdots \\ \hat{i}_{\hat{P}1} & \hat{i}_{\hat{P}2} & \dots & \hat{i}_{\hat{P}F} \end{pmatrix} . \tag{7}$$

We apply the SVD (singular value decomposition) to the image matrix.

$$\hat{\mathbf{I}} = \mathbf{U}\mathbf{W}\mathbf{V}^\top . \tag{8}$$

The rank of image matrix $\hat{\mathbf{I}}$ is 3. Extracting three components from $\hat{P} \times F$ left singular matrix $\mathbf{U}$, $F \times F$ singular value matrix $\mathbf{W}$, $F \times F$ right singular matrix $\mathbf{V}^\top$ results in $\hat{P} \times 3$, 3×3, $3 \times F$ matrices $\mathbf{U}'$, $\mathbf{W}'$, $\mathbf{V}'^\top$, respectively.

$$\mathbf{I} = \mathbf{U}'\mathbf{W}'\mathbf{V}'^\top . \tag{9}$$

Below shows the definition of pseudo surface matrix $\mathbf{S}'$ and pseudo light matrix $\mathbf{L}'$.

$$\mathbf{S}' = \mathbf{U}' , \quad \mathbf{L}' = \mathbf{W}'\mathbf{V}'^\top . \tag{10}$$

These matrices $\mathbf{S}'$ and $\mathbf{L}'$ are not the true surface matrix and the true light matrix. We have to disambiguate an ambiguity exists among $\mathbf{S}'$ and $\mathbf{L}'$, which is represented as matrix $\mathbf{A}$, in order to uniquely determine the true surface matrix $\mathbf{S}$ and the true light matrix $\mathbf{L}$. The ambiguity matrix $\mathbf{A}$ is 3×3 regular matrix which is shown below.

$$\mathbf{S} = \mathbf{S}'\mathbf{A} , \quad \mathbf{L} = \mathbf{A}^{-1}\mathbf{L}' . \tag{11}$$

3.4 Constant albedo constraint

Input image divided by albedo becomes the shading image, thus albedo is constant in shading image. Therefore, we solve the ambiguity matrix $\mathbf{A}$ using the constraint which forces the albedo to be constant. In other words, the reason why we have divided the albedo from input images in Section 3.2 is that we can add the constraint to force the albedo to be constant.

The true surface vector $\mathbf{s}_p$ can be obtained by multiplying the pseudo surface vector $\mathbf{s}'_p$ by the ambiguity matrix $\mathbf{A}$.

$$\mathbf{s}_p^\top = \mathbf{s}'^\top_p \mathbf{A} . \tag{12}$$

The norm of surface vector represents the square of albedo, namely, $\mathbf{s}_p^\top \mathbf{s}_p$ or $\mathbf{s}'^\top_p \mathbf{A}\mathbf{A}^\top \mathbf{s}'_p$. We define symmetrical matrix $\mathbf{B}$ as follows.

$$\mathbf{B} = \mathbf{A}\mathbf{A}^\top = \begin{pmatrix} b_1 & b_4 & b_6 \\ b_4 & b_2 & b_5 \\ b_6 & b_5 & b_3 \end{pmatrix} . \tag{13}$$

Constraint condition that enforces the squared albedo to be one is represented as follows.

$$\mathbf{s}'^\top_p \mathbf{B}\mathbf{s}'_p = 1 . \tag{14}$$

Equation (14) can be reformulated as follows.

$$\begin{pmatrix} s'^2_{xp} & s'^2_{yp} & s'^2_{zp} & 2s'_{xp}s'_{yp} & 2s'_{yp}s'_{zp} & 2s'_{zp}s'_{xp} \end{pmatrix} \cdot$$
$$\begin{pmatrix} b_1 & b_2 & b_3 & b_4 & b_5 & b_6 \end{pmatrix}^\top = 1 . \tag{15}$$

We concatenate Equation (15) for $\hat{P}$ numbers of pixels and form the following equation.

$$\mathbf{C}\mathbf{b} = \mathbf{1} , \tag{16}$$
$$\mathbf{C} = \begin{pmatrix} s'^2_{x1} & s'^2_{y1} & \dots & 2s'_{z1}s'_{x1} \\ s'^2_{x2} & s'^2_{y2} & \dots & 2s'_{z2}s'_{x2} \\ \vdots & \vdots & \ddots & \vdots \\ s'^2_{x\hat{P}} & s'^2_{y\hat{P}} & \dots & 2s'_{z\hat{P}}s'_{x\hat{P}} \end{pmatrix} ,$$
$$\mathbf{b} = \begin{pmatrix} b_1 & b_2 & \dots & b_6 \end{pmatrix}^\top ,$$
$$\mathbf{1} = \begin{pmatrix} 1 & 1 & \dots & 1 \end{pmatrix}^\top .$$

Solving the above produces $\mathbf{b}$.

$$\mathbf{b} = \mathbf{C}^+\mathbf{1} . \tag{17}$$

The symmetrical matrix $\mathbf{B}$ is re-arranged by Equation (13) from $\mathbf{b}$. SVD of $\mathbf{B}$ is formulated as follows since it is a symmetrical matrix.

$$\mathbf{B} = \mathbf{U}_B\mathbf{W}_B\mathbf{U}_B^\top . \tag{18}$$

As a result, the ambiguity matrix $\mathbf{A}$ is calculated as follows from the symmetrical matrix $\mathbf{B}$.

$$\mathbf{A} = \mathbf{U}_B\mathbf{W}_B^{1/2} . \tag{19}$$

We update the pseudo surface matrix $\mathbf{S}'$ and the light matrix $\mathbf{L}'$ as follows using this ambiguity matrix $\mathbf{A}$.

$$\mathbf{S}'' = \mathbf{S}'\mathbf{A} , \quad \mathbf{L}'' = \mathbf{A}^{-1}\mathbf{L}' . \tag{20}$$

However, still there is an ambiguity, and the remaining ambiguity can be represented as the following orthogonal matrix $\mathbf{R}$.

$$\mathbf{S} = \mathbf{S}''\mathbf{R} , \quad \mathbf{L} = \mathbf{R}^\top\mathbf{L}'' . \tag{21}$$

3.5 Constraints using guide normal

Suppose that we have detected the pixel positions of the object boundary in the image plane (Figure 3). Some algorithm may conjecture the approximate shape of the object from the silhouette obtained from a single image. The details of this shape is far from the true shape, however, it is approximately similar to the true shape. We denote such shape obtained from silhouette
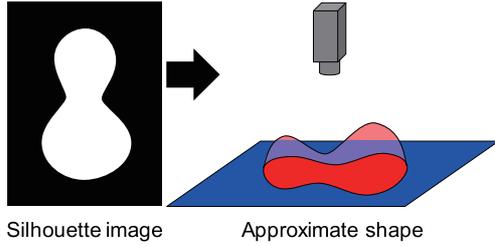
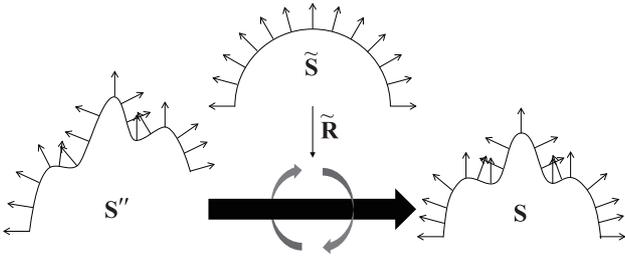Figure 3. Approximate shape obtained from silhouette.

Figure 4. Constraint using guide normal.

(a) Light direction (b) Target object

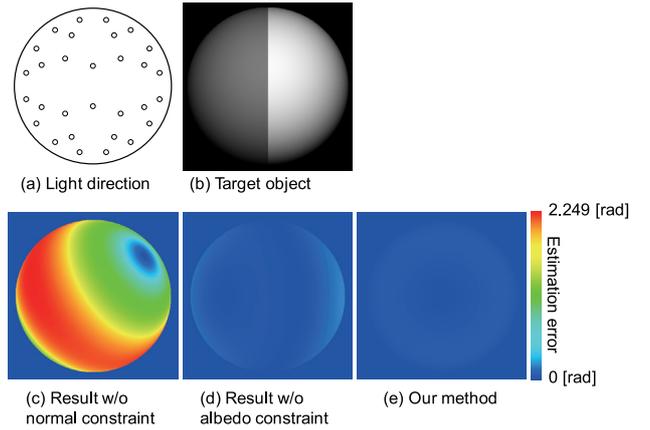(c) Result w/o normal constraint (d) Result w/o albedo constraint (e) Our method

Figure 5. Experimental result [sphere, simulation]: (a) Lighting condition, (b) synthesized sphere, and (c)–(e) estimation error of surface normal. (c) Result if normal constraint is not used, (d) result if albedo constraint is not used, and (e) our method.
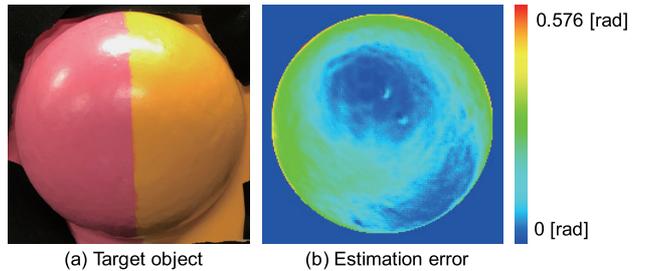

(a) Target object (b) Estimation error

Figure 6. Experimental result [sphere, real]: (a) Real sphere, and (b) estimation error of surface normal.

as guide normal in this paper. We disambiguate Equation (21) using this guide normal. The algorithm to calculate guide normal used in this paper is quite different from other existing methods, however, we skip to explain it since it is a combination of existing techniques developed in the field of image processing. Since the guide normal can be obtained solely from the images, we do not need any other sensors such as laser range sensor.

Since the guide normal is different from true normal, it is still difficult to obtain the true normal. The framework of uncalibrated photometric stereo works effectively in this difficult situation: The guide normal is used solely as the constraint with three degree-of-freedom (Equation (21)), which means that only the approximate shape is constrained by the guide normal while the details of the shape is preserved (Figure 4).

Denoting the guide normal matrix as $\tilde{\mathbf{S}}$, the relation between the updated pseudo surface matrix $\mathbf{S}''$ and the ambiguity orthogonal matrix $\mathbf{R}$ can be represented as follows.

$$\tilde{\mathbf{S}} = \mathbf{S}''\mathbf{R}. \qquad (22)$$

As a result, $\mathbf{R}$ is obtained.

$$\mathbf{R} = \mathbf{S}''^{+}\tilde{\mathbf{S}}. \qquad (23)$$

After that, we orthogonalize $\mathbf{R}$ and obtain the orthogonal matrix $\tilde{\mathbf{R}}$. Finally, we obtain the surface matrix and the light matrix as follows.

$$\mathbf{S} = \mathbf{S}''\tilde{\mathbf{R}}, \quad \mathbf{L} = \tilde{\mathbf{R}}^{\top}\mathbf{L}''. \qquad (24)$$

Although we have obtained $\hat{P}$ numbers of pixels which satisfies Equation (6), we have not yet obtained P numbers of pixels of the whole image. Therefore, we again calculate the surface matrix $\mathbf{S}$ from the light matrix $\mathbf{L}$.

4 Experimental results

We capture multiple images under different position of single light source, while the camera and the target object are fixed. Additional sensors are not required.

First of all, we show the results applied to a sphere, since the true surface normal of sphere can be ideally calculated thus it is adequate for evaluation. Figure 5 (b) is one of the input image of the ideal sphere synthesized under the light direction shown in Figure 5 (a). Our method (Figure 5 (e)) use both the surface normal constraint (Section 3.5) and the albedo constraint

(a) Target object (b) Guide albedo (c) Estimation error

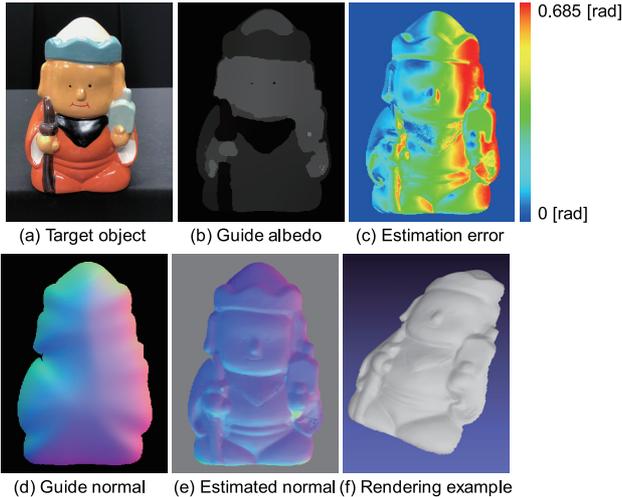(d) Guide normal (e) Estimated normal (f) Rendering example

Figure 7. Experimental result [buddha]: (a) Target object, (b) estimated intrinsic image (reflectance), (c) estimation error, (d) guide normal, (e) estimated normal, and (f) rendering example.

(a) Target object (b) Guide albedo (c) Estimation error

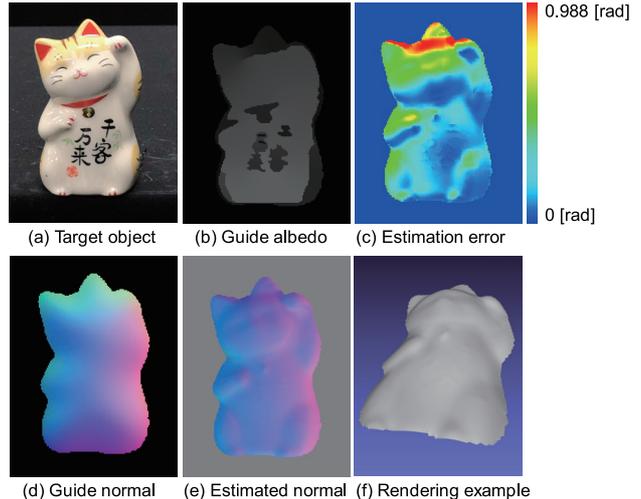(d) Guide normal (e) Estimated normal (f) Rendering example

Figure 8. Experimental result [cat]: (a) Target object, (b) estimated intrinsic image (reflectance), (c) estimation error, (d) guide normal, (e) estimated normal, and (f) rendering example.

(Section 3.2). Figure 5 (e) shows the estimation error of surface normal, whose average error is 0.105 [rad]. If we do not use the guide normal, the error is quite large which is 1.58 [rad], as is shown in Figure 5 (c). The error if we do not use the guide albedo is 0.110 [rad], and the error is nonuniform affected by the albedo difference as is shown in Figure 5 (d). Figure 6 (b) is the result of the real sphere (Figure 6 (a)), and its average error is 0.152 [rad]. While the error of the calibrated photometric stereo distorts the shape locally, the error of the uncalibrated photometric stereo distorts the shape globally.

The results of buddha object and cat object are shown in Figures 7 and 8, respectively. Either has multiple albedos, and thus these objects are difficult to treat with uncalibrated photometric stereo. In Figures 7–8, (a), (b), (c), (d), (e), and (f) represent the target object, the guide albedo, the estimation error, the guide normal, the surface normal obtained by our method, and the rendering example. As for calculating the estimation error (Figure 7 (c) and Figure 8 (c)), the surface normal calculated by conventional photometric stereo (calibrated photometric stereo) is used as the ground truth. Compared to the guide normal whose details are not reproduced, our method reproduces the details of the shape.

5 Conclusion

We proposed an uncalibrated photometric stereo which use intrinsic image which represents the albedo and guide normal which represents the approximated shape as constraints. Without using any other sensors such as laser range sensors, we calculated the hypothesized albedo and normal solely from image sequences. We have verified not only theoretically but also experimentally that these two constraints can solve the problem of uncalibrated photometric stereo.

References

[1] N. G. Alldrin, S. P. Mallick, and D. J. Kriegman, "Resolving the generalized bas-relief ambiguity by entropy minimization," in *Proceedings of IEEE Conference on Computer Vision and Pattern Recognition*, 2007.

[2] H. G. Barrow and J. M. Tennenbaum, "Recovering intrinsic scene characteristics from images," in *A. Hanson and R. Riseman, editors, Computer Vision Systems*, Academic Press, pp. 3–26, 1978.

[3] R. Basri, D. Jacobs, and I. Kemelmacher, "Photometric stereo with general, unknown lighting," *International Journal of Computer Vision*, vol. 72, no. 3, pp. 239–257, 2007.

[4] P. N. Belhumeur, D. J. Kriegman, and A. L. Yuille, "The bas-relief ambiguity," *International Journal of Computer Vision*, vol. 35, no. 1, pp. 33–44, 1999.

[5] M. K. Chandraker, F. Kahl, and D. J. Kriegman, "Reflections on the generalized bas-relief ambiguity," in

Proceedings of IEEE Conference on Computer Vision and Pattern Recognition, pp. 788–795, 2005.

[6] O. Drbohlav and R. Šára, "Specularities reduce ambiguity of uncalibrated photometric stereo," in *Proceedings of European Conference on Computer Vision*, pp. 46–62, 2002.

[7] P. Favaro and T. Papadhimitri, "A closed-form solution to uncalibrated photometric stereo," in *Proceedings of IEEE Conference on Computer Vision and Pattern Recognition*, 2012.

[8] G. D. Finlayson, S. D. Hordley, and M. S. Drew, "Removing shadows from images," in *Proc. of European Conf. on Computer Vision*, vol. 4, pp. 823–836, 2002.

[9] A. S. Georghiades, "Incorporating the Torrance and Sparrow model of reflectance in uncalibrated photometric stereo," in *Proceedings of IEEE International Conference on Computer Vision*, pp. 816–825, 2003.

[10] H. Hayakawa, "Photometric stereo under a light source with arbitrary motion," *Journal of the Optical Society of America A*, vol. 11, no. 11, pp. 3079–3089, 1994.

[11] S. Ikehata, D. Wipf, Y. Matsushita, and K. Aizawa, "Photometric stereo using sparse Bayesian regression for general diffuse surfaces," *IEEE Transactions on Pattern Analysis and Machine Intelligence*, vol. 39, no. 9, pp. 1816–1831, 2014.

[12] R. Kimmel, M. Elad, D. Shaked, B. Keshet, and I. Sobel, "A variational framework for retinex," *International Journal of Computer Vision*, vol. 52, no. 1, pp. 7–23, 2003.

[13] E. H. Land, "The Retinex theory of color vision," in *Scientific American*, vol. 237, no. 6, p. 108–128, 1977.

[14] Y. Matsushita, K. Nishino, K. Ikeuchi, and M. Sakauchi, "Illumination normalization with time-dependent intrinsic images for video surveillance," in *Conf. on Computer Vision and Pattern Recognition*, vol. 1, pp. 3–10, 2003.

[15] D. Miyazaki and K. Ikeuchi, "Photometric stereo under unknown light sources using robust SVD with missing data," in *Proceedings of IEEE International Conference on Image Processing*, pp. 4057–4060, 2010.

[16] T. Mori, R. Taketa, S. Hiura, and K. Sato, "Photometric linearization by robust PCA for shadow and specular removal," *Computer Vision, Imaging and Computer Graphics. Theory and Application*, vol. 359, pp. 211–224, 2013.

[17] Y. Mukaigawa, Y. Ishii, and T. Shakunaga, "Analysis of photometric factors based on photometric linearization," *Journal of the Optical Society of America A*, vol. 24, no. 10, pp. 3326–3334, 2007.

[18] I. Sato, T. Okabe, Q. Yu, and Y. Sato, "Shape reconstruction based on similarity in radiance changes under varying illumination," in *Proceedings of International Conference on Computer Vision*, 2007.

[19] B. Shi, Y. Matsushita, Y. Wei, C. Xu, and P. Tan, "Self-calibrating photometric stereo," in *Proceedings of IEEE Conference on Computer Vision and Pattern Recognition*, pp. 1118–1125, 2010.

[20] H.-Y. Shum, K. Ikeuchi, and R. Reddy, "Principal component analysis with missing data and its application to polyhedral object modeling," *IEEE Transactions on Pattern Analysis and Machine Intelligence*, vol. 17, no. 9, pp. 854–867, 1995.

[21] M. F. Tappen, W. T. Freeman, and E. H. Adelson, "Recovering intrinsic images from a single image," in *Advances in Neural Information Processing Systems*, MIT Press, 2002.

[22] R. Tibshirani, "Regression shrinkage and selection via the lasso," *Journal of the Royal Statistics Society B*, vol. 58, pp. 267–288, 1996.

[23] C. Tomasi and T. Kanade, "Shape and motion from image streams under orthography: A factorization method," *International Journal of Computer Vision*, vol. 9, no. 2, pp. 137–154, 1992.

[24] Y. Weiss, "Deriving intrinsic images from image sequences," in *Proc. of 9th IEEE Int'l Conf. on Computer Vision*, pp. 63–75, 2001.

[25] R. J. Woodham, Y. Iwahori, and R. A. Barman, "Photometric stereo: Lambertian reflectance and light sources with unknown direction and strength," in *Technical Report*, 1991.

[26] L. Wu, A. Ganesh, B. Shi, Y. Matsushita, Y. Wang, and Y. Ma, "Robust photometric stereo via low-rank matrix completion and recovery," in *Computer Vision - ACCV 2010*, vol. 6494, pp. 703–717, 2010.

[27] Z. Wu and P. Tan, "Calibrating photometric stereo by holistic reflectance symmetry analysis," in *Proc. of IEEE Conference on Computer Vision and Pattern Recognition*, 2013.

[28] A. L. Yuille, D. Snow, R. Epstein, and P. N. Belhumeur, "Determining generative models of objects under varying illumination: Shape and albedo from multiple images using SVD and integrability," *International Journal of Computer Vision*, vol. 35, no. 3, pp. 203–222, 1999.

[29] M. Zhipeng, B. Shi, F. Lu, S. Yeing, and Y. Matsushita, "Uncalibrated photometric stereo under natural illumination," in *International Conference on Computer Vision and Pattern Recognition*, pp. 2936–2945, 2018.